

# Hyperpolarizability of Plasmonic Meta-Atoms in Metasurfaces

M. Saad Bin-Alam, Joshua Baxter, Kashif M. Awan, Antti Kiviniemi, Yaryna Mamchur, Antonio Calà Lesina, Kosmas L. Tsakmakidis, Mikko J. Huttunen, Lora Ramunno, and Ksenia Dolgaleva\*

Cite This: *Nano Lett.* 2021, 21, 51–59

Read Online

ACCESS |

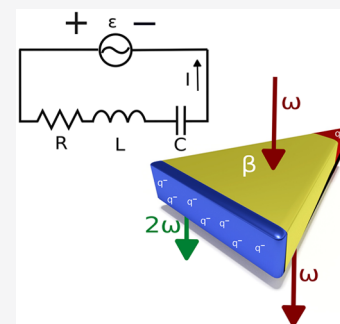
Metrics & More

Article Recommendations

Supporting Information

**ABSTRACT:** Plasmonic metasurfaces are promising as enablers of nanoscale nonlinear optics and flat nonlinear optical components. Nonlinear optical responses of such metasurfaces are determined by the nonlinear optical properties of individual plasmonic meta-atoms. Unfortunately, no simple methods exist to determine the nonlinear optical properties (hyperpolarizabilities) of the meta-atoms hindering the design of nonlinear metasurfaces. Here, we develop the equivalent *RLC* circuit (resistor, inductor, capacitor) model of such meta-atoms to estimate their second-order nonlinear optical properties, that is, the first-order hyperpolarizability in the optical spectral range. In parallel, we extract from second-harmonic generation experiments the first-order hyperpolarizabilities of individual meta-atoms consisting of asymmetrically shaped (elongated) plasmonic nanoprisms, verified with detailed calculations using both nonlinear hydrodynamic-FDTD and nonlinear scattering theory. All three approaches, analytical, experimental, and computational, yield results that agree very well. Our empirical *RLC* model can thus be used as a simple tool to enable an efficient design of nonlinear plasmonic metasurfaces.

**KEYWORDS:** Plasmonics, Meta-atoms, Nonlinear Optics, Hyperpolarizability, Anharmonic *RLC* oscillator



Photonic metamaterials are artificial structures exhibiting optical properties that in natural materials are either very weak or entirely lacking. Among these properties are phase mismatched light-propagation, optical magnetism, strong chirality, and epsilon-near-zero behavior.<sup>1–5</sup> There is a growing interest in understanding and harnessing the nonlinear optical responses of metasurfaces.<sup>6–14</sup> Many photonic applications including frequency conversion, THz generation, photon-pair generation, ultrashort-pulse generation, frequency-comb generation, and all-optical switching<sup>15–19</sup> rely on nonlinear optics occurring in large bulky devices where one must contend with phase mismatching. In contrast, the small footprint of metasurfaces virtually guarantees phase matching, and moreover, the nonlinear emission can be precisely controlled.<sup>2,3,20,21</sup>

Plasmonic metasurfaces have recently emerged as a promising candidate for enabling nanoscale nonlinear optics.<sup>6</sup> The optical responses of plasmonic meta-atoms serving as unit cells of metasurfaces are dictated by the collective movement of the conduction electrons giving rise to localized surface plasmons (LSPs). Therefore, it is imperative to investigate the conduction electron dynamics and the nonlinear response of the constituting meta-atoms. Such investigations can be performed, for example, by using the hydrodynamic plasma model<sup>22–25</sup> and the nonlinear scattering theory.<sup>26</sup> However, relying on computational tools is not always convenient due to their complexity and the large amount of computational resources they often require.

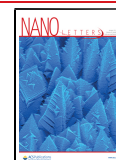
Linear and nonlinear optical responses of plasmonic meta-atoms can also be predicted by equivalent *RLC* circuit

(resistor, inductor, capacitor) theory.<sup>27–31</sup> This approach has correctly described the nonlinear and magnetic responses of split-ring resonators operating at microwave frequencies.<sup>32</sup> Nevertheless, it remained unclear whether the *RLC* approach could describe conduction electron dynamics in plasmonic meta-atoms adequately enough to accurately predict their nonlinear responses at optical wavelengths as well. In this Letter, we derive the first-order hyperpolarizability of individual plasmonic meta-atoms by adapting the equivalent *RLC* model that we find can, indeed, be used to predict collective second-order nonlinear responses of large metasurfaces. First, we derive an expression for the first-order hyperpolarizability with an unknown nonlinear coefficient *a* that represents the strength of the nonlinear charge oscillation in an individual meta-atom. Our goal is to determine the value of *a* through physical arguments and to validate our approach through rigorous experiments and numerical calculations. Next, we describe our second-harmonic generation (SHG) experiments, where we measured SHG emission from metasurfaces consisting of randomly arranged gold elongated nanoprisms. From these measurements, we extract the

Received: July 21, 2020

Revised: December 17, 2020

Published: December 24, 2020



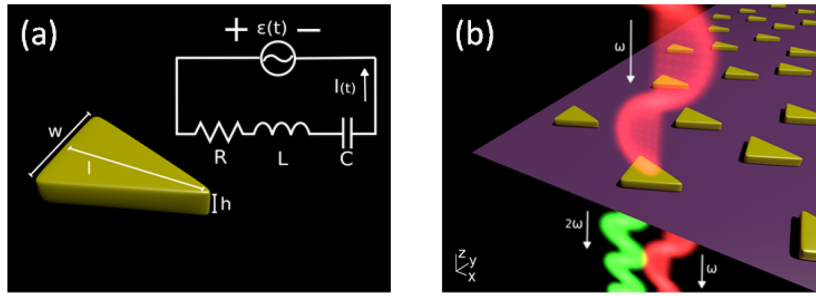


**Figure 1.** An artist's depiction of (a) an equivalent  $RLC$  circuit diagram for the investigated nanoprisms, and (b) metasurface consisting of a random array of elongated gold nanoprisms.

spectrum of their first-order hyperpolarizability. This result is then validated by two sets of finite-difference time domain (FDTD) calculations. In the first, the material nonlinearities are directly implemented within the code via a nonlinear hydrodynamic plasma model. The second is based on nonlinear scattering theory where the experimentally determined second-order nonlinear permittivity of gold is used.

Finally, we present a simple empirical derivation for the unknown  $RLC$ -model nonlinear coefficient  $a$ , which we then use to perform an order-of-magnitude estimate of the first-order hyperpolarizability. Our intuitive physical interpretation of  $a$  is such that the  $RLC$  circuit model we present can be extended to describe metasurfaces with different meta-atoms without requiring a priori experimental validation. This simple analytical tool, capable of predicting the hyperpolarizabilities of meta-atoms based on their shapes, dimensions, and material compositions, will prove indispensable in the realization of metasurfaces with tailored nonlinear optical responses.

Because of its resonant nature, a plasmonic meta-atom behaves as an  $RLC$  circuit, illustrated in Figure 1a, whose dynamics can be described via<sup>32</sup>

$$L\dot{\tilde{I}} + R\tilde{I} + \tilde{V}_C(\tilde{q}) = \tilde{\varepsilon}(t) \quad (1)$$

where  $\tilde{I}$  is the free charge current,  $L$  is the distributed inductance,  $R$  is the distributed resistance, and  $\tilde{V}_C$  is the induced voltage due to the effective capacitance  $C$  of the circuit. We use a tilde to represent time-varying quantities and an overdot to represent time derivatives.

The free charges of a rodlike plasmonic meta-atom, in the presence of an incident field  $\tilde{E}_{\text{inc}} = E_0 \exp(-i\omega t)$  polarized along its length  $l$ , will accumulate at a facet resulting in a charge separation and an effective capacitance  $C$ . The incident field drives the  $RLC$  circuit by creating an electromotive force, which in the dipole approximation, takes the form  $\tilde{\varepsilon} = \tilde{E}_{\text{inc}}l$ . The dynamics of the free charge is described by the current  $\tilde{q} = \tilde{I}$ , where  $\pm q$  is the induced charge at opposing facets of the nanostructure. We assume that the nonlinearity is sufficiently weak, allowing us to write the nonlinear voltage as<sup>32</sup>

$$V_C(\tilde{q}) = (\tilde{q} + a\tilde{q}^2)/C \quad (2)$$

where  $a$  quantifies the strength of the nonlinearity. Note that the nonlinear perturbation we assumed here is valid at least up to  $\sim 10$  GW/cm<sup>2</sup> incident field intensities.<sup>33</sup> Inserting these expressions into eq 1, we obtain

$$\ddot{\tilde{q}} + 2\gamma\dot{\tilde{q}} + \omega_0^2\tilde{q} + a\omega_0^2\tilde{q}^2 = C\omega_0^2l\tilde{E}_{\text{inc}} \quad (3)$$

where  $\omega_0 = 1/\sqrt{LC}$  is the resonance frequency of the circuit and  $\gamma = R/2L$  is the free-electron damping constant of

metals.<sup>32</sup> This model accounts for the dispersive nature of metals by implicitly considering a Drude model with  $\gamma$  in eq 3 and  $\omega_p$  in eq 10b which are given for gold in Methods.<sup>32</sup> The  $RLC$  model is valid in the same wavelength ranges as the Drude model. Typically for plasmonics, this is when the pump wavelength is in the infrared.

When the excitation wavelengths are close to the LSP resonance of the meta-atom, the conduction electron dynamics are well described using the  $RLC$  approach.<sup>28</sup> A steady-state solution to eq 3 is found by implementing perturbation theory<sup>34</sup>

$$\tilde{q} = \frac{C\omega_0^2l}{D(\omega)}E_{\text{inc}}e^{-i\omega t} - \frac{aC^2\omega_0^6l^2}{D^2(\omega)D(2\omega)}E_{\text{inc}}^2e^{-i2\omega t} \quad (4)$$

where  $D(\omega') = (\omega_0^2 - \omega'^2 - 2i\gamma\omega')$ . We write the total induced dipole moment as  $\tilde{p} = \tilde{q}l$ , and recall that the dipole moment can be expressed in the frequency domain as<sup>34</sup>

$$p = \epsilon_0\alpha E_{\text{inc}} + \epsilon_0\beta E_{\text{inc}}^2 \quad (5)$$

where  $\alpha$  is the linear polarizability and  $\beta$  is the first-order hyperpolarizability of the meta-atom. Combining eqs 4 and 5, we obtain

$$\alpha(\omega) = -\frac{C\omega_0^2l^2}{\epsilon_0D(\omega)} \quad (6a)$$

$$\beta(2\omega; \omega) = -a\frac{C^2\omega_0^6l^3}{\epsilon_0D(2\omega)D^2(\omega)} \quad (6b)$$

As the lengths of the meta-atoms can be a significant fraction of the exciting wavelength, higher-order multipoles can be excited, and one must consider this possibility in general, especially for nonlinear emission at shorter wavelengths.<sup>35</sup> However, in this study our goal is to create a model that gives an order of magnitude estimate of SHG emission, and we therefore consider only the electric dipole term. The hyperpolarizability in eq 6b can be considered an "effective" hyperpolarizability that helps us to achieve this goal. In what follows, we use experimentally and computationally derived hyperpolarizability spectra to determine a quantitative value for the nonlinear coefficient  $a$ .

We first need to consider a geometry for our meta-atom. SHG is a coherent second-order nonlinear process, and therefore, very sensitive to the symmetry of the object under investigation.<sup>34</sup> In fact, centrosymmetric-shaped structures exhibit very weak electric-dipole SHG responses<sup>36</sup> (see also Figure S1 in Supporting Information Section S1). Nanostructures with low symmetry, such as split-ring resonators, L-

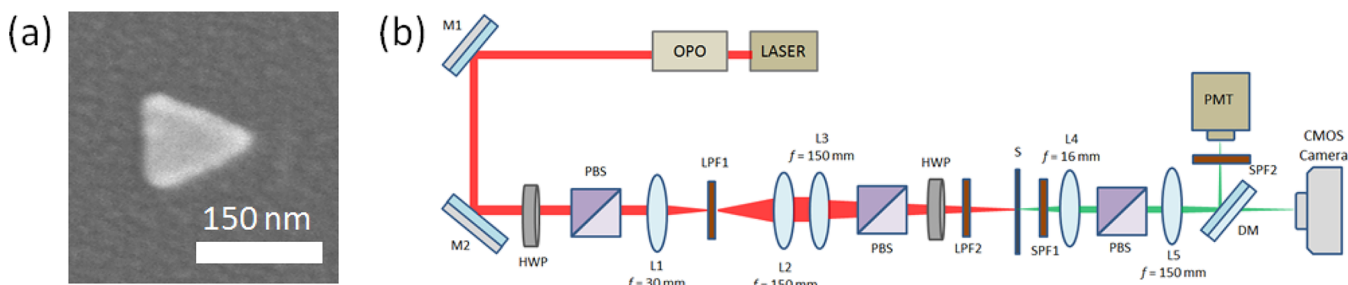


**Figure 2.** (a) Representative scanning electron micrograph of a fabricated gold nanoprism. (b) Schematic of the nonlinear SHG experimental setup (details in ref 36).

shapes, or nanoprisms exhibit a stronger second-order response, and consequently are especially interesting in studies of even-order nonlinear optical effects.<sup>36–38</sup> We therefore study elongated triangular nanoprisms due to their low symmetry and simple geometrical shapes.

We now determine the hyperpolarizability through experiments. Four metasurfaces containing gold nanoprisms with widths of  $w = 100$  nm, thicknesses of  $h = 20$  nm, and lengths of  $l = 145, 156, 167,$  and  $178$  nm were fabricated on a fused silica substrate using electron beam lithography, thermal evaporation, and a standard metal lift-off procedure.<sup>39</sup> In order to minimize interparticle coupling effects occurring in periodic arrays,<sup>40–46</sup> each metasurface consisted of 10 000 identical, randomly positioned nanoprisms (oriented in the same direction) deposited into an area of  $200 \times 200 \mu\text{m}^2$ . This allowed us to investigate ensemble responses that have spectral features identical to the responses of individual meta-atoms.<sup>47</sup> The arrangement is schematically represented in Figure 1b, while a representative scanning electron micrograph of an individual nanoprism is shown in Figure 2a. Alternatively, individual meta-atoms could be investigated by using nonlinear microscopy.<sup>48</sup>

The transmission spectra of the four metasurfaces are shown in Figure 3a. To verify successful fabrication of the metasurfaces, we compared the measured spectra with those obtained from FDTD (see Methods) [see Figure 3b]. In order for the simulated nanoprism to closely resemble the actual fabricated meta-atoms, we rounded its corners with a circle of 15 nm radius. The LSP resonances of simulated nanoprisms for  $l = 145, 156, 167,$  and  $178$  nm peaked at 1030, 1080, 1120, and 1170 nm, respectively, which are in good agreement with the measurements.

We performed SHG experiments using the setup shown in Figure 2b (described in detail elsewhere<sup>36</sup>). A laser beam originating from an optical parametric oscillator (Chameleon Compact) was used to illuminate the sample metasurfaces. The optical parametric oscillator was pumped with a Ti:sapphire laser (Chameleon Vision II), generating 200 fs long pulses with a repetition rate of 82 MHz. The average power of the signal beam was kept at 8 mW to avoid potential sample damage via accumulative heating. The SHG emission from the metasurfaces was detected as a function of fundamental wavelength ranging from 1000–1300 nm using a power-calibrated photomultiplier tube [see Figure 3c]. The input-beam polarization was set to be linear and aligned with the long axes of the nanoprisms.

We verified the calibration of our setup to provide order-of-magnitude estimates for the first-order hyperpolarizabilities  $\beta$ . This was achieved by measuring SHG emission from a 0.5

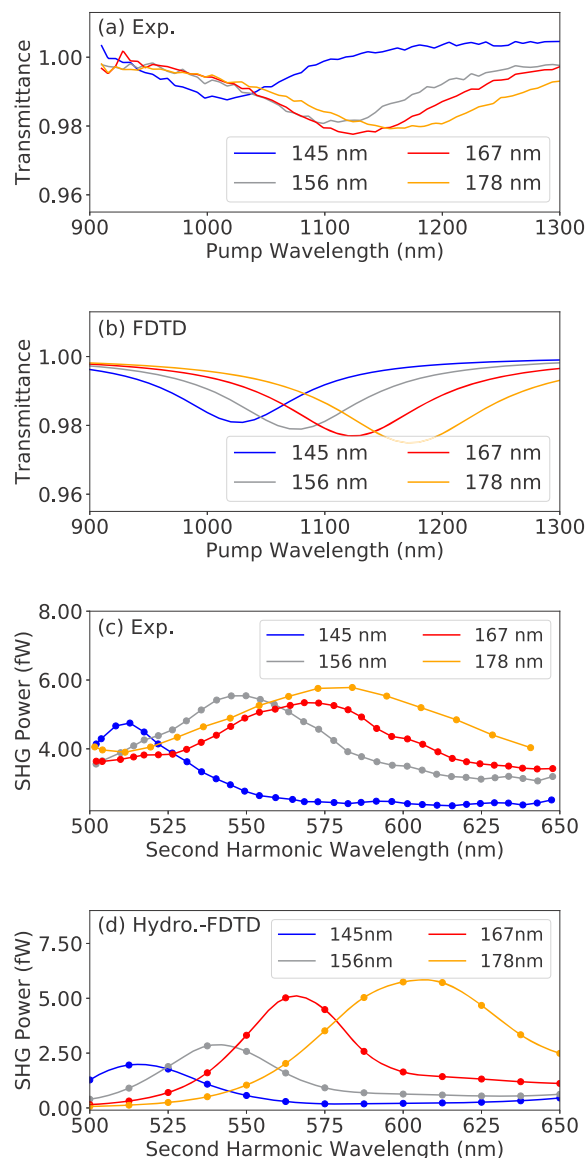


**Figure 3.** Measured (a) and calculated (b) transmission spectra of random arrays of elongated gold nanoprisms of different lengths  $l$  along the direction of the light polarization ( $l = 145, 156, 167,$  and  $178$  nm). Measured (c) and calculated (d) SHG emission intensity as a function of second-harmonic wavelength for the same four metasurfaces.

mm-thick Y-cut quartz crystal and using the model described in ref 49 to estimate the second-order susceptibility  $\chi^{(2)}$  value

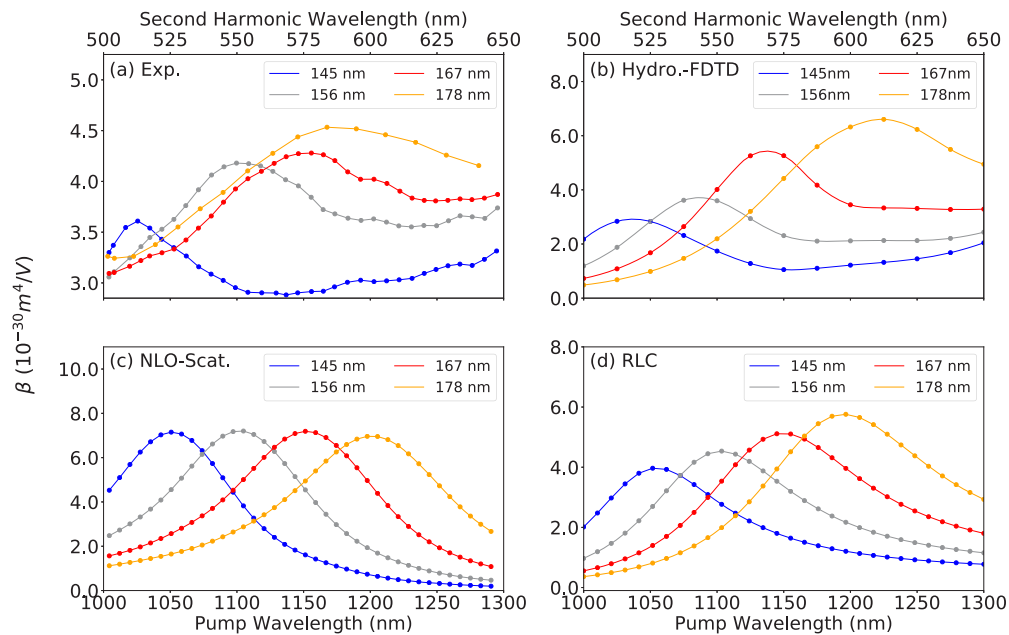


**Figure 4.** (a) Experimentally extracted values of  $\beta$  for the investigated nanoprisms. Corresponding values of  $\beta$ , predicted by (b) hydrodynamic-FDTD, (c) nonlinear scattering theory, and (d) the introduced nonlinear RLC model.

for the quartz crystal. Our estimate ( $\chi_{xxx}^{(2)} = 0.53$  pm/V) is in excellent agreement with the literature.<sup>34</sup>

To estimate the values of  $\beta$  for the nanoprisms from the experimental data, we calculated the macroscopic  $\chi^{(2)}$  using the same approach as we used for quartz.<sup>49</sup> We estimated the meta-atom number density of the metasurfaces to be  $n = 10\,000/(200\ \mu\text{m} \times 200\ \mu\text{m} \times 20\ \text{nm}) = 1.25 \times 10^{19}\ \text{m}^{-3}$ , then linked the detected SHG intensities to the hyperpolarizabilities using the relation  $\beta = \chi^{(2)}/n$ . The extracted values of  $\beta$  as a function of the incident fundamental wavelength are plotted for the four investigated nanoprisms in Figure 4a.

Next we wish to determine the hyperpolarizability using numerical computations via the hydrodynamic plasma model.<sup>22–25</sup> This was used in conjunction with the two-critical-points model<sup>50</sup> for gold in an in-house 3D-FDTD code.<sup>51</sup> As the metasurface contains randomly positioned nanoprisms, periodic boundary conditions could not be used to simplify the calculation. Further, the metasurfaces were too large for a single FDTD simulation. We therefore developed a new method for quantitative approximation of the power. First, we calculated the nonlinear scattered power in the forward direction of a single nanoprism resulting from a Gaussian pulse with duration and peak intensity as in the experiments. For each nanoprism in the random metasurface, the forward-scattered power was scaled to the laser field incident on that particular nanoprism. The individual powers from all nanoprisms in the metasurface were then incoherently summed. The calculated second-harmonic power spectrum, shown in Figure 3d shows excellent quantitative agreement with experimental measurements.

To estimate  $\beta$  using the hydrodynamic plasma model, we first calculate the nonlinear scattered power from a single nanoprism by integrating the nonlinear scattering spectrum from a single pulse and multiplying it by the repetition rate of the laser. If the nonlinear scattered power  $P_{\text{NL}}$  was purely from a dipole, we can approximate the magnitude of nonlinear dipole moment  $|p|$  by  $|p|^2 = 12\pi P_{\text{NL}}/(nc_0^2 Z_0 k_0^4)$ ,<sup>52</sup> where  $c_0$  is the speed of light in vacuum,  $k_0$  is the vacuum wavenumber,  $Z_0$  is

the vacuum impedance, and  $n$  is the refractive index of the surrounding medium. We calculate  $\beta$  using eq 5 and plot it in Figure 4b. One can see excellent quantitative and qualitative agreement between the simulation and experimental results.

Finally we use another numerical approach based on the nonlinear scattering theory<sup>53,54</sup> to determine the nonlinear coefficient  $a$ . Though not as rigorous as the hydrodynamic plasma model, it is a simpler and more computationally efficient technique for calculating nonlinear emission from nanostructures. Because the SHG emission was detected only in one direction, and the detector was in the far-field, we were able to use the Lorentz reciprocity theorem.<sup>26,55</sup> First, we obtained the local field distributions for both the fundamental and SHG wavelengths of interest via linear simulations. The excitation field was assumed to be a normally incident plane wave polarized along the long axis of the nanoprism. The dimensions of the simulated nanoprism were matched with the experimental values, and the sharp corners of the meta-atoms were again rounded.

Then we calculated the generated nonlinear source polarization present on the surface of the meta-atom, where we used the experimentally extracted local nonlinear susceptibility values for gold.<sup>56</sup> The local field was transformed into the surface coordinate system by reconstructing the surface of the meta-atom by using a Delaunay triangulation mesh and performing subsequent field interpolation onto that surface. Once the nonlinear surface polarization was calculated, we used the Lorentz reciprocity theorem to predict the emitted SHG field from the meta-atom (in the forward direction) by calculating the mode overlap integral between the SHG source polarization and the local field distribution at the SHG wavelength.<sup>26,57</sup> The last step was to use eq 5 to calculate  $\beta$ . The values of  $\beta$  are plotted in Figure 4c and agree in resonance position and in the order-of-magnitude values with the experimental and hydrodynamic plasma model results.

Now that we have obtained agreement for the values of  $\beta$  from the experimental data and the two numerical approaches, we can estimate the value of the nonlinear coefficient  $a$

required for the *RLC* model from eq 6b. We find that  $a \approx 10^{14} \text{ C}^{-1}$ , and plot eq 6b, our *RLC* model prediction, in Figure 4d.

While we are confident in the order of magnitude of  $a$ , it was quite labor intensive to obtain. We now present a physically intuitive explanation for the order of magnitude of  $a$  that we have obtained. In the discussion surrounding Miller's rule presented by Boyd,<sup>34</sup> it is argued that for a bulk material, the linear and nonlinear restoring forces felt by an electron are comparable in magnitude when the charge displacement is approximately equal to the interatomic spacing  $d$ . This is then used to estimate the strength of the nonlinear restoring force.

In contrast, the polarization of a meta-atom results from an accumulation of free charge on the surface. The charge buildup occurs at the facet within a thin layer with thickness on the order of the Fermi wavelength ( $\lambda_F \approx 0.5 \text{ nm}$  for gold). In the absence of external fields, the density of free electrons in this layer would be  $n_0$ , the equilibrium free electron density, and thus there is no excess charge at the surface.

In the presence of an external field, it is reasonable to assume that at most two electrons (with different spins) can reside within  $\lambda_F$  of each other. This would lead to a surface charge density of

$$\sigma \approx \pm en_0 \lambda_F \quad (7)$$

where the sign depends on which side of the meta-atom is being considered. Under this condition one would expect the linear and nonlinear responses to be comparable, in a similar spirit to ref 34; in fact,  $\lambda_F \approx d$ , the interatomic spacing in gold. From eq 2, the linear and nonlinear terms of  $V_C$  are equal when  $\tilde{q} = a\tilde{q}^2$ , giving  $a = 1/\tilde{q}$ , where  $\tilde{q} = \sigma A$  and  $A$  is the surface area containing  $\sigma$  on one side of the meta-atom.

For the nanoprisms considered in this paper, our simulations showed that the region over which there is significant charge density covers a perimeter of approximately 100 nm both at the tip end and at the base end. Given the height of the nanoprism is 20 nm, we obtain

$$a = \frac{1}{en_0 A \lambda_F} = 1.1 \times 10^{14} \text{ C}^{-1} \quad (8)$$

where  $n_0 = 5.9 \times 10^{28} \text{ m}^{-3}$  in gold. This is remarkably close to what the detailed simulations and measurements predict.

It is also worth mentioning that from the *RLC* model we can obtain the ratio

$$\frac{\beta(2\omega, \omega)}{\alpha^2(\omega)\alpha(2\omega)} = \frac{ae_0^2}{Cl^3} \quad (9)$$

which is, in essence, a form of Miller's rule for meta-atoms. It is frequency independent and only depends on the geometry of the particle. This is similar to the anharmonic oscillator model of ref 34 where the ratios of the susceptibility functions are also only dependent on the effective mass and the number density of the electrons.

From Figure 4, we see that all four approaches yield values of  $\beta$  within the same order of magnitude  $\sim 10^{-30} \text{ m}^4/\text{V}$ . This agreement is very encouraging because it has been notoriously difficult to make quantitative predictions of nonlinear optical processes occurring in plasmonic materials.<sup>9,36</sup> The simpler methods (*RLC* and nonlinear scattering theory), though predicting the correct spectral peak positions, are missing some features that are visible in the experimental results and hydrodynamic calculation, such as the oscillations at longer wavelengths. These features are believed to be caused by a

secondary resonance of the nanoprisms and interband transitions in gold.

Despite the great amount of previous work on nonlinear metasurfaces, only a handful of investigations have provided order-of-magnitude estimates of meta-atom's hyperpolarizabilities.<sup>35,58–61</sup> Our values of hyperpolarizability are 2–3 orders of magnitude smaller than previous estimates of somewhat similar meta-atoms; this discrepancy is not unexpected, because the experimental setups, the wavelength ranges considered, and the investigated meta-atoms have all been different. While we investigated the coherent SHG emission, earlier investigations measured incoherent hyper-Rayleigh scattering (HRS) signals, and estimated the values of  $\beta$  indirectly by comparing the HRS signals from meta-atoms with HRS signals measured from known solvents. Furthermore, the earlier HRS experiments performed at shorter excitation wavelengths than what we considered. Because the interband transitions of gold start playing a role at wavelengths shorter than 550 nm,<sup>62</sup> these earlier-extracted hyperpolarizability values may have contained an additional contribution arising from the interband transitions.<sup>34</sup>

Our results also demonstrate the usefulness of the nonlinear *RLC* approach. Although simple and intuitive, it describes the dynamics of conduction electrons adequately enough to predict the strength of nonlinear optical responses of plasmonic meta-atoms. Nonlinear *RLC* model had earlier been found to accurately describe nonlinear responses of metamaterials at the microwave wavelengths.<sup>32</sup> We show here that it can be adapted for optical wavelengths as well. This model can also be applied to meta-atoms of any other geometry made of any other plasmonic material, which will be demonstrated in an upcoming publication.

To conclude, we have derived a nonlinear equivalent *RLC* circuit model that can be used to quickly and accurately predict the nonlinear optical responses of meta-atoms in the visible and near-IR spectral ranges. We fabricated four metasurfaces consisting of randomly positioned gold nanoprisms and characterized their second-harmonic generation emissions. We compared the experimental results with the predictions based on the hydrodynamic plasma model, nonlinear scattering theory, and our nonlinear *RLC* model. All of the results were found to be in good agreement. Our *RLC* approach provides new insights into understanding the nonlinear responses of meta-atoms and opens new possibilities for application-oriented efficient nonlinear metasurface design.<sup>36,38,63–66</sup>

## ■ METHODS

**Parameters for the Nonlinear *RLC* Model.** In order to find the expressions for the capacitance  $C$  and inductance  $L$  for an elongated nanoprism [shown in Figure 1a], we first calculated the capacitance  $C$  and inductance  $L$  of a rectangular nanobar from its geometrical dimensions using the following formulas

$$C = \pi \epsilon_0 \epsilon_r r_0 \quad (10a)$$

$$L = \frac{\mu_0 l}{2\pi} \log \frac{4l}{h} + \frac{\mu_0 l}{\frac{\omega_p^2}{c_0^2} wh} \quad (10b)$$

In eq 10a, the capacitance  $C$  can be defined as the electric charge divided by the potential difference between the two facets of a rectangular nanobar (similar to ref 28 for a plasmonic cylindrical nanorod).

To keep similarity with the formula for  $C$  given in ref 28, we assumed  $r_0 \approx 10^{-9}$  nm in eq 10a as a constant parameter mimicking the radius of a cylinder encircling the nanobar. However, due to the geometrical difference between the cylinder and rectangular nanobar, we slightly modified eq 10b for the inductance  $L$  to match the LSPR spectral position with the simulation and experimental linear transmission data.

In eq 10b, the self-inductance is given by

$$L_{\text{self}} = \frac{\mu_0 l}{2\pi} \log \frac{4l}{h} \quad (11)$$

the kinetic inductance is given by

$$L_{\text{kinetic}} = \frac{\mu_0 l}{\frac{\omega_p^2}{c_0^2} wh} \quad (12)$$

$\epsilon_0$  is the vacuum permittivity ( $8.85 \times 10^{-12}$  F/m), the relative permittivity of glass is  $\epsilon_r \approx 3.9$ ,  $\mu_0$  is the vacuum permeability ( $1.257 \times 10^{-6}$  H/m),  $\omega_p = 13.8 \times 10^{15}$  rad/s is the plasma frequency for gold in the optical regime,<sup>67</sup> and  $c_0 = 3 \times 10^8$  m/s is the speed of light in vacuum.

**Simulations. Linear FDTD Simulations.** Linear FDTD simulations were performed to calculate the linear transmission spectra of the metasurface using an in-house FDTD solver.<sup>51</sup> The spectra were calculated by subtracting the absorption and backscattering cross sections of all the meta-atoms on the metasurface from the total area of the metasurface. The transmission spectrum is then  $T = (A_{\text{metasurface}} - (A_{\text{back-scatt}} + A_{\text{abs}})) / A_{\text{metasurface}}$ . The cross-sectional data is calculated from a single meta-atom and scaled by the number of meta-atoms on the metasurface. A standard total-field/scattered-field layout is used to calculate the cross sections and the simulation domain is truncated by convolutionally perfectly matched layers. The linear Drude +2 critical points model<sup>50</sup> is used for the optical properties of gold and accounts for contributions from the conduction electrons and interband transitions. A broadband raised cosine pulse<sup>51</sup> is used as a source excitation.

**Hydrodynamic FDTD Simulations.** Hydrodynamic FDTD calculations were conducted using the same in-house FDTD solver. The simulation setup is identical to that used in the linear transmission spectra, except that the hydrodynamic model (solved via centered finite differences) replaces the Drude model (in the Drude +2 critical points model), and the source excitation is replaced with a 200 fs Gaussian pulse centered at wavelengths ranging from 1000 to 1300 nm. All simulations using the in-house FDTD solver were run on the Graham cluster operated by Compute Canada.<sup>68</sup>

**Nonlinear Scattering Theory.** The nonlinear response of a meta-atom was estimated also by using calculations based on the nonlinear scattering theory and the Lorentz reciprocity theorem.<sup>26,57</sup> The strength of the SHG emission in the direction of interest was evaluated by calculating a mode overlap integral over the fundamental excitation and SHG emission modes. The relevant field profiles for the fundamental and SHG fields were calculated using the Lumerical FDTD software, and the mode overlap integrals were calculated numerically using Matlab. In the FDTD simulations the optical constant of gold was taken from ref 67. The fields on the surface of the meta-atom were estimated by using Delaunay triangulation, and only the surface contributions were considered when calculating the nonlinear response of the gold.<sup>56</sup>

**Fabrication.** We used 2 cm  $\times$  2 cm fused silica chips as substrates. The chips were coated with bilayer electron-beam resist, consisting of 50 nm thick PMMA with a molecular weight of 495 k as the bottom layer and 25 nm thick PMMA with a molecular weight of 950 k as the top resist layer. The plasmonic nanostructures were then patterned using 30 kV Raith electron-beam lithography system (CRPuO, uOttawa) with a dose of 550  $\mu\text{C}/\text{cm}^2$ . The patterned resist was then developed for 2 min in 3:1 MIBK/IPA (methyl isobutyl ketone/isopropyl alcohol), followed by depositing a 20 nm layer of gold by electron-beam evaporation and, finally, a lift-off by immersion in acetone. A computer-aided layout of a randomly arranged elongated nanoprism array that was used to create the resist mask and a schematic of the fabrication process flow are shown in Figure S2 and Figure S3, respectively, in Supporting Information Sections S2 and S3. More details are described in ref 39.

**Characterization. Linear Characterization.** Linear transmission spectra of the samples were measured using a collimated tungsten-halogen light source (experimental setup is shown in Figure S4 in the Supporting Information Section S4). The incident polarization was controlled using a broadband linear polarizing filter. The entire sample was illuminated, and the transmission from a single device was measured by first using a lens to image the sample plane into an intermediate image plane. The transmission from the correct device was then selected by a translating a variable aperture in this image plane, and by using a second lens to guide the transmitted light into the spectrometer.

**Nonlinear Characterization.** Signal beam from an optical parametric oscillator (Chameleon Compact) was used to illuminate the sample metasurfaces using a spectral SHG setup described in Supporting Information Section S5 (shown in Figure S5). The optical parametric oscillator was pumped using a Ti:sapphire laser (Chameleon Vision II) generating 200 fs long pulses with a repetition rate of 82 MHz. The average power of the signal beam was kept at 8 mW to avoid potential sample damage via accumulative heating. The SHG emission from the metasurfaces was detected as a function of the fundamental wavelength ranging between 1000 and 1300 nm using a power-calibrated photomultiplier tube (see Figure S5 in the Supporting Information Section S5). The input beam polarization was set to be linear and aligned with the long axes of the nanoprisms.

## ■ ASSOCIATED CONTENT

### Supporting Information

The Supporting Information is available free of charge at <https://pubs.acs.org/doi/10.1021/acs.nanolett.0c02991>.

Symmetric and nonsymmetric nanostructures' SHG response, computer-aided design of the layout of the randomly oriented elongated nanoprisms, plasmonic metasurface fabrication process, experimental setup for linear transmittance measurement, details of nonlinear experimental setup (PDF)

## ■ AUTHOR INFORMATION

### Corresponding Author

Ksenia Dolgaleva – School of Electrical Engineering and Computer Science, University of Ottawa, Ottawa, Ontario K1N 6N5, Canada; Department of Physics, University of

Ottawa, Ottawa, Ontario K1N 6N5, Canada;  
Email: ksenia.dolgaleva@uottawa.ca

## Authors

**M. Saad Bin-Alam** – School of Electrical Engineering and Computer Science, University of Ottawa, Ottawa, Ontario K1N 6N5, Canada; [orcid.org/0000-0002-0208-4004](https://orcid.org/0000-0002-0208-4004)

**Joshua Baxter** – Department of Physics, University of Ottawa, Ottawa, Ontario K1N 6N5, Canada; [orcid.org/0000-0002-1498-9361](https://orcid.org/0000-0002-1498-9361)

**Kashif M. Awan** – Stewart Blusson Quantum Matter Institute, University of British Columbia, Vancouver, British Columbia V6T 1Z4, Canada; School of Electrical Engineering and Computer Science, University of Ottawa, Ottawa, Ontario K1N 6N5, Canada

**Antti Kiviniemi** – Laboratory of Photonics, Tampere University, FI-33014 Tampere, Finland

**Yaryna Mamchur** – National Technical University of Ukraine, “Igor Sikorsky Kyiv Polytechnic Institute”, 03056 Kyiv, Ukraine; School of Electrical Engineering and Computer Science, University of Ottawa, Ottawa, Ontario K1N 6N5, Canada

**Antonio Calà Lesina** – Hannover Centre for Optical Technologies, Cluster of Excellence PhoenixD (Photonics, Optics, and Engineering – Innovation Across Disciplines), and Fakultät für Maschinenbau (Institut für Transport- und Automatisierungstechnik), Leibniz Universität Hannover, 30167 Hannover, Germany; [orcid.org/0000-0002-9384-6245](https://orcid.org/0000-0002-9384-6245)

**Kosmas L. Tsakmakidis** – Section of Condensed Matter Physics, Department of Physics, National and Kapodistrian University of Athens, Panepistimioupolis, GR-157 84 Athens, Greece

**Mikko J. Huttunen** – Laboratory of Photonics, Tampere University, FI-33014 Tampere, Finland

**Lora Ramunno** – Department of Physics, University of Ottawa, Ottawa, Ontario K1N 6N5, Canada

Complete contact information is available at:  
<https://pubs.acs.org/10.1021/acs.nanolett.0c02991>

## Author Contributions

K.D. conceived the basic idea for the whole work. K.L.T. conceived the idea of implementing the RLC model. M.S.B.-A. derived the analytical nonlinear RLC model. K.M.A. fabricated the metasurface substrate. M.J.H., M.S.B.-A., and A.K. carried out the measurements. J.B. performed the linear and nonlinear hydrodynamic-FDTD model simulations. J.B. and L.R. derived an expression for the nonlinear coefficient  $a$  using intuitive arguments. Y.M. made the illustration. K.D., L.R., M.J.H., K.L.T., and A.C.L. supervised the research and the development of the manuscript. M.S.B.A., J.B., and M.J.H. wrote the first draft of the manuscript. All coauthors subsequently took part in the revision process and approved the final copy of the manuscript.

## Notes

The authors declare no competing financial interest.

## ACKNOWLEDGMENTS

The authors thank Robert W. Boyd, Ekaterina Poutrina, John E. Sipe, and Gerd Leuchs for their valuable feedback and suggestions. The authors also thank Martti Kauranen for providing his lab at Tampere University in Finland to perform

the experiment. K.D. and L.R. acknowledge support from the Canada Research Chairs (CRC) Program. K.D. acknowledges the financial support of the Natural Sciences and Engineering Research Council of Canada (NSERC) Discovery program. M.S.B.-A. acknowledges the support of the Ontario Graduate Scholarship (OGS), the University of Ottawa Excellence Scholarship, and the University of Ottawa International Experience Scholarship. J.B. acknowledges the financial support of NSERC Canada Graduate Scholarship-Master's (CGSM) Program and the University of Ottawa Excellence Scholarship, and the computational resources of Compute Canada. M.J.H. acknowledges the support of the Academy of Finland (Grant 308596) and the Flagship of Photonics Research and Innovation (PREIN) funded by the Academy of Finland (Grant 320165). K.L.T. acknowledges support from the General Secretariat for Research and Technology (GSRT) and the Hellenic Foundation for Research and Innovation (HFRI) under Grant 1819. A.C.L. acknowledges the Bundesministerium für Bildung und Forschung (German Federal Ministry of Education and Research) under the Tenure-Track Programme, and the Deutsche Forschungsgemeinschaft (DFG, German Research Foundation) under Germany's Excellence Strategy within the Cluster of Excellence PhoenixD (EXC 2122, Project ID 390833453).

## REFERENCES

- (1) Kildishev, A. V.; Boltasseva, A.; Shalae, V. M. Planar photonics with metasurfaces. *Science* **2013**, *339*, 1232009.
- (2) Yu, N.; Genevet, P.; Kats, M. A.; Aieta, F.; Tetienne, J.-P.; Capasso, F.; Gaburro, Z. Light propagation with phase discontinuities: generalized laws of reflection and refraction. *Science* **2011**, *334*, 333–337.
- (3) Alù, A.; Silveirinha, M. G.; Salandrino, A.; Engheta, N. Epsilon-near-zero metamaterials and electromagnetic sources: Tailoring the radiation phase pattern. *Phys. Rev. B: Condens. Matter Mater. Phys.* **2007**, *75*, 155410.
- (4) Zhang, S.; Park, Y.-S.; Li, J.; Lu, X.; Zhang, W.; Zhang, X. Negative index in chiral metamaterials. *Phys. Rev. Lett.* **2009**, *102*, 023901.
- (5) Soukoulis, C. M.; Wegener, M. Past achievements and future challenges in the development of three-dimensional photonic metamaterials. *Nat. Photonics* **2011**, *5*, 523.
- (6) Kauranen, M.; Zayats, A. V. Nonlinear plasmonics. *Nat. Photonics* **2012**, *6*, 737–748.
- (7) Lapine, M.; Shadrivov, I. V.; Kivshar, Y. S. Colloquium: Nonlinear metamaterials. *Rev. Mod. Phys.* **2014**, *86*, 1093–1123.
- (8) Minovich, A. E.; Miroshnichenko, A. E.; Bykov, A. Y.; Murzina, T. V.; Neshev, D. N.; Kivshar, Y. S. Functional and nonlinear optical metasurfaces. *Laser & Photonics Reviews* **2015**, *9*, 195–213.
- (9) Butet, J.; Brevet, P. F.; Martin, O. J. Optical Second Harmonic Generation in Plasmonic Nanostructures: From Fundamental Principles to Advanced Applications. *ACS Nano* **2015**, *9*, 10545–10562.
- (10) Li, G.; Zhang, S.; Zentgraf, T. Nonlinear photonic metasurfaces. *Nat. Rev. Mater.* **2017**, *2*, 1–14.
- (11) Rahimi, E.; Gordon, R. Nonlinear Plasmonic Metasurfaces. *Adv. Opt. Mater.* **2018**, *6*, 1800274.
- (12) Keren-Zur, S.; Michaeli, L.; Suchowski, H.; Ellenbogen, T. Shaping light with nonlinear metasurfaces. *Adv. Opt. Photonics* **2018**, *10*, 309–353.
- (13) Pertsch, T.; Kivshar, Y. Nonlinear optics with resonant metasurfaces. *MRS Bull.* **2020**, *45*, 210–220.
- (14) Lesina, A. C.; Berini, P.; Ramunno, L. Origin of third harmonic generation in plasmonic nanoantennas. *Optical Materials Express*. *Opt. Mater. Express* **2017**, *7*, 1575–1580.

- (15) Kwiat, P. G.; Mattle, K.; Weinfurter, H.; Zeilinger, A.; Sergienko, A. V.; Shih, Y. New high-intensity source of polarization-entangled photon pairs. *Phys. Rev. Lett.* **1995**, *75*, 4337.
- (16) Rasekh, P.; Saliminabi, M.; Yildirim, M.; Boyd, R. W.; Ménard, J.-M.; Dolgaleva, K. Propagation of broadband THz pulses: effects of dispersion, diffraction and time-varying nonlinear refraction. *Opt. Express* **2020**, *28*, 3237–3248.
- (17) Brabec, T.; Krausz, F. Intense few-cycle laser fields: Frontiers of nonlinear optics. *Rev. Mod. Phys.* **2000**, *72*, 545.
- (18) Kippenberg, T. J.; Holzwarth, R.; Diddams, S. A. Microresonator-Based Optical Frequency Combs. *Science* **2011**, *332*, 555–560.
- (19) Shcherbakov, M. R.; Vabishchevich, P. P.; Shorokhov, A. S.; Chong, K. E.; Choi, D. Y.; Stauda, I.; Miroschnichenko, A. E.; Neshev, D. N.; Fedyanin, A. A.; Kivshar, Y. S. Ultrafast All-Optical Switching with Magnetic Resonances in Nonlinear Dielectric Nanostructures. *Nano Lett.* **2015**, *15*, 6985–6990.
- (20) Minerbi, E.; Keren-Zur, S.; Ellenbogen, T. Nonlinear metasurface fresnel zone plates for terahertz generation and manipulation. *Nano Lett.* **2019**, *19*, 6072–6077.
- (21) Lin, Z.; Huang, L.; Xu, Z. T.; Li, X.; Zentgraf, T.; Wang, Y. Four-Wave Mixing Holographic Multiplexing Based on Nonlinear Metasurfaces. *Adv. Opt. Mater.* **2019**, *7*, 1900782.
- (22) Sipe, J. E.; So, V. C. Y.; Fukui, M.; Stegeman, G. I. Analysis of second-harmonic generation at metal surface. *Phys. Rev. B: Condens. Matter Mater. Phys.* **1980**, *21*, 4389.
- (23) Scalora, M.; Vincenti, M. A.; De Ceglia, D.; Roppo, V.; Centini, M.; Akozbek, N.; Bloemer, M. J. Second- and third-harmonic generation in metal-based structures. *Phys. Rev. A: At., Mol., Opt. Phys.* **2010**, *82*, 1–14.
- (24) Ciraci, C.; Poutrina, E.; Scalora, M.; Smith, D. R. Second-harmonic generation in metallic nanoparticles: Clarification of the role of the surface. *Phys. Rev. B: Condens. Matter Mater. Phys.* **2012**, *86*, 1–10.
- (25) Ginzburg, P.; Krasavin, A. V.; Wurtz, G. A.; Zayats, A. V. Nonperturbative hydrodynamic model for multiple harmonics generation in metallic nanostructures. *ACS Photonics* **2015**, *2*, 8–13.
- (26) O'Brien, K.; Suchowski, H.; Rho, J.; Salandrino, A.; Kante, B.; Yin, X.; Zhang, X. Predicting nonlinear properties of metamaterials from the linear response. *Nat. Mater.* **2015**, *14*, 379–383.
- (27) Engheta, N.; Salandrino, A.; Alu, A. Circuit Elements at Optical Frequencies: Nanoinductors, Nanocapacitors, and Nanoresistors. *Phys. Rev. Lett.* **2005**, *95*, 095504.
- (28) Huang, C.-p.; Yin, X.-g.; Huang, H.; Zhu, Y.-y. Study of plasmon resonance in a gold nanorod with an LC circuit model. *Opt. Express* **2009**, *17*, 6407.
- (29) Zhou, J.; Koschny, T.; Kafesaki, M.; Economou, E. N.; Pendry, J. B.; Soukoulis, C. M. Saturation of the Magnetic Response of Split-Ring Resonators at Optical Frequencies. *Phys. Rev. Lett.* **2005**, *95*, 223902.
- (30) Tretyakov, S. On geometrical scaling of split-ring and double-bar resonators at optical frequencies. *Metamaterials* **2007**, *1*, 40–43.
- (31) Staffaroni, M.; Conway, J.; Vedantam, S.; Tang, J.; Yablonovitch, E. Circuit analysis in metal-optics. *Photonics Nanostructures - Fundam. Appl.* **2012**, *10*, 166–176.
- (32) Poutrina, E.; Huang, D.; Smith, D. R. Analysis of nonlinear electromagnetic metamaterials. *New J. Phys.* **2010**, *12*, 093010.
- (33) Lippitz, M.; Van Dijk, M. A.; Orrit, M. Third-harmonic generation from single gold nanoparticles. *Nano Lett.* **2005**, *5*, 799–802.
- (34) Boyd, R. W. *Nonlinear optics*, 4th ed.; Academic Press: San Diego, 2020.
- (35) Butet, J.; Duboiset, J.; Bachelier, G.; Russier-Antoine, I.; Benichou, E.; Jonin, C.; Brevet, P. F. Optical second harmonic generation of single metallic nanoparticles embedded in a homogeneous medium. *Nano Lett.* **2010**, *10*, 1717–1721.
- (36) Czaplicki, R.; Kiviniemi, A.; Huttunen, M. J.; Zang, X.; Stolt, T.; Vartiainen, I.; Butet, J.; Kuittinen, M.; Martin, O. J. F.; Kauranen, M. Less is more – enhancement of second-harmonic generation from metasurfaces by reduced nanoparticle density. *Nano Lett.* **2018**, *18*, 7709–7714.
- (37) Klein, M. W.; Enkrich, C.; Wegener, M.; Linden, S. Second-harmonic generation from magnetic metamaterials. *Science* **2006**, *313*, 502–504.
- (38) Huttunen, M. J.; Rasekh, P.; Boyd, R. W.; Dolgaleva, K. Using surface lattice resonances to engineer nonlinear optical processes in metal nanoparticle arrays. *Phys. Rev. A: At., Mol., Opt. Phys.* **2018**, *97*, 053817.
- (39) Awan, K. *Fabrication of III-V Integrated Photonic Devices*. Ph.D. Thesis, Université d'Ottawa/University of Ottawa, Ottawa, 2018.
- (40) Auguie, B.; Barnes, W. L. Collective resonances in gold nanoparticle arrays. *Phys. Rev. Lett.* **2008**, *101*, 143902.
- (41) Meinzer, N.; Barnes, W. L.; Hooper, I. R. Plasmonic meta-atoms and metasurfaces. *Nat. Photonics* **2014**, *8*, 889–898.
- (42) Kataja, M.; Hakala, T. K.; Julku, A.; Huttunen, M. J.; van Dijken, S.; Törmä, P. Surface lattice resonances and magneto-optical response in magnetic nanoparticle arrays. *Nat. Commun.* **2015**, *6*, 7072.
- (43) Huttunen, M. J.; Dolgaleva, K.; Törmä, P.; Boyd, R. W. Ultra-strong polarization dependence of surface lattice resonances with out-of-plane plasmon oscillations. *Opt. Express* **2016**, *24*, 28279.
- (44) Kravets, V. G.; Kabashin, A. V.; Barnes, W. L.; Grigorenko, A. N. Plasmonic Surface Lattice Resonances: A Review of Properties and Applications. *Chem. Rev.* **2018**, *118*, 5912–5951.
- (45) Reshef, O.; Saad-Bin-Alam, M.; Huttunen, G.; Carlow, M.; Sullivan, B. T.; Ménard, J.-M.; Dolgaleva, K.; Boyd, R. W. Multiresonant High-Q Plasmonic Metasurfaces. *Nano Lett.* **2019**, *19*, 6429–6434.
- (46) Bin-Alam, M. S.; Reshef, O.; Mamchur, Y.; Alam, M. Z.; Carlow, G.; Upham, J.; Sullivan, B. T.; Ménard, J.-M.; Huttunen, M. J.; Boyd, R. W.; Dolgaleva, K. Ultra-high-Q resonances in plasmonic metasurfaces. *arXiv* 2020, <https://arxiv.org/abs/2004.05202v2> (accessed July 10, 2020).
- (47) Shi, L.; Hakala, T. K.; Rekola, H. T.; Martikainen, J.-P.; Moerland, R. J.; Torma, P. Spatial Coherence Properties of Organic Molecules Coupled to Plasmonic Surface Lattice Resonances in the Weak and Strong Coupling Regimes. *Phys. Rev. Lett.* **2014**, *112*, 153002.
- (48) Bautista, G.; Huttunen, M. J.; Mäkitalo, J.; Kontio, J. M.; Simonen, J.; Kauranen, M. Second-harmonic generation imaging of metal nano-objects with cylindrical vector beams. *Nano Lett.* **2012**, *12*, 3207–3212.
- (49) Herman, W. N.; Hayden, L. M. Maker fringes revisited: second-harmonic generation from birefringent or absorbing materials. *J. Opt. Soc. Am. B* **1995**, *12*, 416.
- (50) Prokopoulos, K. P.; Zografopoulos, D. C. A Unified FDTD/PML Scheme Based on Critical Points for Accurate Studies of Plasmonic Structures. *J. Lightwave Technol.* **2013**, *31*, 2467–2476.
- (51) Lesina, A. C.; Vaccari, A.; Berini, P.; Ramunno, L. On the convergence and accuracy of the FDTD method for nanoplasmonics. *Opt. Express* **2015**, *23*, 10481–10497.
- (52) Jackson, J. D. *Classical electrodynamics*, 3rd ed.; John Wiley: New York, 1999.
- (53) de Beer, A. G. F.; Roke, S.; Dadap, J. I. Theory of optical second-harmonic and sum-frequency scattering from arbitrarily shaped particles. *J. Opt. Soc. Am. B* **2011**, *28*, 1374–1384.
- (54) Mäkitalo, J.; Suuriniemi, S.; Kauranen, M. Boundary element method for surface nonlinear optics of nanoparticles: erratum. *Opt. Express* **2013**, *21*, 10205.
- (55) Roke, S.; Bonn, M.; Petukhov, A. V. Nonlinear optical scattering: The concept of effective susceptibility. *Phys. Rev. B: Condens. Matter Mater. Phys.* **2004**, *70*, 1–10.
- (56) Wang, F. X.; Rodríguez, F. J.; Albers, W. M.; Ahorinta, R.; Sipe, J. E.; Kauranen, M. Surface and bulk contributions to the second-order nonlinear optical response of a gold film. *Phys. Rev. B: Condens. Matter Mater. Phys.* **2009**, *80*, 4–7.

(57) De Beer, A. G.; Roke, S. Nonlinear Mie theory for second-harmonic and sum-frequency scattering. *Phys. Rev. B: Condens. Matter Mater. Phys.* **2009**, *79*, 1–9.

(58) Vance, F. W.; Lemon, B. I.; Hupp, J. T. Enormous Hyper-Rayleigh Scattering from Nanocrystalline Gold Particle Suspensions. *J. Phys. Chem. B* **1998**, *102*, 10091–10093.

(59) Russier-antoine, I.; Jonin, C.; Nappa, J.; Benichou, E.; Brevet, P. F. Wavelength dependence of the hyper Rayleigh scattering response from gold nanoparticles. *J. Chem. Phys.* **2004**, *120*, 10748.

(60) Nappa, J.; Revillod, G.; Russier-Antoine, I.; Benichou, E.; Jonin, C.; Brevet, P. F. Electric dipole origin of the second harmonic generation of small metallic particles. *Phys. Rev. B: Condens. Matter Mater. Phys.* **2005**, *71*, 165407.

(61) Duboisset, J.; Russier-Antoine, I.; Benichou, E.; Bachelier, G.; Jonin, C.; Brevet, P. F. Single Metallic Nanoparticle Sensitivity with Hyper Rayleigh Scattering. *J. Phys. Chem. C* **2009**, *113*, 13477–13481.

(62) Novotny, L.; Hecht, B. *Principles of nano-optics*, 1st ed.; Cambridge University Press: New York, 2006.

(63) Michaeli, L.; Keren-Zur, S.; Avayu, O.; Suchowski, H.; Ellenbogen, T. Nonlinear Surface Lattice Resonance in Plasmonic Nanoparticle Arrays. *Phys. Rev. Lett.* **2017**, *118*, 970.

(64) Huttunen, M. J.; Reshef, O.; Stolt, T.; Dolgaleva, K.; Boyd, R. W.; Kauranen, M. Efficient nonlinear metasurfaces by using multiresonant high-Q plasmonic arrays. *Journal of the Optical Society of America B* **2019**, *36*, 118.

(65) Chen, S.; Reineke, B.; Li, G.; Zentgraf, T.; Zhang, S. Strong nonlinear optical activity induced by lattice surface modes on plasmonic metasurface. *Nano Lett.* **2019**, *19*, 6278–6283.

(66) Hooper, D. C.; Kuppe, C.; Wang, D.; Wang, W.; Guan, J.; Odom, T. W.; Valev, V. K. Second harmonic spectroscopy of surface lattice resonances. *Nano Lett.* **2019**, *19*, 165–172.

(67) Johnson, P. B.; Christy, R. W. Optical Constants of the Noble Metals. *Phys. Rev. B - Condens. Matter Mater. Phys.* **1972**, *6*, 4370.

(68) Graham - CC Doc. <https://docs.computecanada.ca/wiki/Graham> (accessed Sept. 4, 2019).